Materials Today Communications 24 (2020) 101259

Contents lists available at ScienceDirect

Materials Today Communications

journal homepage: www.elsevier.com/locate/mtcomm

First-principles study of mechanical and optical properties for $ZnS_{1-x}O_x$ alloying compounds

Junfu Qi[a], Yuefeng Yin[b,*], Xiangdong Ding[a], Jun Sun[a], Junkai Deng[a,*]

[a] State Key Laboratory for Mechanical Behavior of Materials, Xi'an Jiaotong University, Xi'an 710049, China
[b] Department of Materials Science and Engineering, Monash University, Victoria 3800, Australia

ARTICLE INFO

Keywords:
$ZnS_{1-x}O_x$
Infrared window
Mechanical properties
Optical properties
Vacancy

ABSTRACT

An excellent infrared window material should have both high transmittance and good mechanical strength to adapt to applications in harsh environments. In this report, we use first-principles calculations to investigate the effect of oxygen alloying on the mechanical and optical properties of the well-used infrared window material ZnS. We have found that with increasing oxygen content, the mechanical properties including elastic constants, bulk modulus, shear modulus, Young's modulus of $ZnS_{1-x}O_x$ compounds are improved compared to the pristine phase. Meanwhile, the infrared optical transmittance of the system is retained with changing oxygen compositions. We have also considered the influence of oxygen/sulfur vacancy defects in the system. We have observed that the optical transmittance of the system is degraded upon induction of vacancies. These results have revealed that the mechanical properties of optical materials can be effectively enhanced with appropriate alloying, but there are also challenges in practice due to the presence of defects. Our investigations can guide the design of these infrared optical materials in special applications such as aircraft and space systems.

1. Introduction

Excellent optical materials require good robustness to be used in harsh environments [1–3]. However, the infrared transmitting performance is often degraded when the mechanical strength of an optical film is improved for conventional commercial materials such as single-crystal sodium chloride and potassium bromide [4,5]. Therefore, there has been a continuing search for robust infrared window materials that can endure harsh outdoor environments with resistance to liquid, solid particle, and thermal stress [5]. Many potential materials have been studied so far, including Ge, GaS, diamond, ZnS, and ZnSe, etc. [2,4,6–9]. However, most of them have either failed to meet optical requirements for applications such as Ge and GaS with narrow spectral range and low infrared transmittance [2,6,7], or faced significant challenges in production technology such as diamonds [2]. Currently, ZnS and ZnSe are still the material-of-choice for infrared window applications due to the combination of longwave infrared transmission window (8–14 μm wavelength), thermal stability, and reasonable mechanical strength [4].

ZnS and ZnSe are semiconducting compounds exhibiting superior infrared transmittance than other candidate materials in two-color infrared windows and strong bulk modulus [4]. ZnS and ZnSe have already been widely used in mid-infrared and far-infrared applications including infrared lenses, laser windows, and infrared night cameras [2,4,10,11]. In particular, ZnS plays a vital role in being used as infrared windows and lenses in particular applications of missile domes and spaceborne systems [11]. However, with the speeds of missile and space aircraft growing faster, the mechanical strength of the infrared window material needs to be further enhanced. Alloying is an effective and economical approach to tackle this challenge. Previous reports have already shown that ZnS_xSe_{1-x} compounds could achieve higher mechanical strength and retain similar infrared transparent performance compared to pristine ZnSe [12–14]. These studies inspires us to investigate whether alloying of other VIA elements such as oxygen could further strengthen the ZnS material without sacrificing excellent optical responses.

In this paper, we systematically investigate the mechanical and optical properties for zinc-blende $ZnS_{1-x}O_x$ by using the first-principles calculations, where the values of x are 0, 0.03(1/32), 0.06(2/32), 0.09(3/32), 0.13(4/32), 0.16(5/32), 0.25(8/32), 0.50(16/32) and 1. In this study, we mainly sample $x < 0.2$, *i.e.*, ZnS with low level of oxygen alloying as we focus on the effect of oxygen doping in ZnS. We have investigated the effect of oxygen alloying concentration in the system. We show that the presence of oxygen in the system could increase the mechanical strength of the system while preserving the optical properties. Moreover, we have examined the impact of sulfur and oxygen

* Corresponding authors.
E-mail addresses: yuefeng.yin@monash.edu (Y. Yin), junkai.deng@mail.xjtu.edu.cn (J. Deng).

https://doi.org/10.1016/j.mtcomm.2020.101259
Received 9 April 2020; Received in revised form 16 May 2020; Accepted 17 May 2020
Available online 21 May 2020

vacancy defects on the properties of the $ZnS_{1-x}O_x$ system. The vacancy study reveals the importance of controlling and reducing defects in practical applications.

2. Computational method

We used first-principles calculations as implemented in the Vienna Ab-initio Simulation Package (VASP) to calculate the structural, mechanical, optical, and electronic properties of $ZnS_{1-x}O_x$ alloying system [15]. The Perdew–Burke–Ernzerhof (PBE) functional under generalized gradient approximation (GGA) was used to describe the exchange and correlation effects [16]. We also used the local density approximation (LDA) functional of the Ceperley-Alder form as parameterized by Perdew and Zunger for comparison [17,18]. The pseudopotentials are generated by the PAW method [19,20]. The cut-off energy for the plane-wave basis was set as 400 eV, and Monkhorst-Pack gamma-centered k-points grid of dimensions 7 × 7 × 7 was adopted for the ZnS or ZnO unit cell. These parameters can provide sufficient numerical accuracy for this study. The equivalent density of k-points mesh was used for $ZnS_{1-x}O_x$ supercells. All structures were relaxed until the ionic forces are smaller than 0.01 eV/ Å. The fully relaxed structures were used for calculations of mechanical and optical properties.

In order to model the $ZnS_{1-x}O_x$alloying system, the special quasi-random structure (SQS) method was implemented in the Alloy Theoretic Automated Toolkit (ATAT) to construct the disordered structures of $ZnS_{1-x}O_x$ compound [21–23]. The disordered supercells were simulated using 64-atoms SQS structures, which represent the best periodic supercell approximation to the true disordered state for a given number of atoms per supercell.

3. Results and discussion

3.1. Structural and mechanical properties

For ZnS applied in infrared window materials, the most energetically stable zinc-blende structure with the space group of F-43M is adopted [11,24]. The zinc-blende structure is also used as the base for all ZnS structure with doped oxygen atoms ($ZnS_{1-x}O_x$ compounds). For fully doped scenario ($x = 1$, *i.e.* ZnO), we also used the zinc blende phase to present a continuous evolution of properties. The zinc blende ZnO can be synthesized in a stable form experimentally and can be used in electronic devices [25,26]. We first investigate the defect-free unit cell of ZnS and ZnO, as shown in Fig. 1(a) and (b). The relaxed lattice constants are 5.44 Å for ZnS and 4.63 Å for ZnO, respectively, based on PBE functional. For comparison, the relaxed lattice constants are determined as 5.30 Å for ZnS and 4.50 Å for ZnO according to LDA functional. We found that the lattice constants obtained *via* PBE functional agree better with experimental values (5.41 Å for ZnS and 4.62 Å for ZnO) than LDA [27,28]. Therefore, in the remaining part of the report, we only present the structural, mechanical, and optical properties based on PBE functional.

As the $ZnS_{1-x}O_x$ alloying compounds had been successfully synthesized by solution-combustion approach [29], we use SQS scheme to construct $ZnS_{1-x}O_x$ crystal structures for different alloying compositions [23]. Fig. 1(c) shows a typical SQS structure of $ZnS_{0.5}O_{0.5}$. The obtained lattice constants of $ZnS_{1-x}O_x$ are plotted against O fraction x in Fig. 2(a), which are all near the blue dashed line. That is with the increase of the O content, the lattice constants of $ZnS_{1-x}O_x$ decrease linearly, which is well consistent with Vegard's law [30]:

$$a_{ZnS_xO_{1-x}} = xa_{ZnO} + (1-x)a_{ZnS} \quad (1)$$

Where a_{ZnO} and a_{ZnS} are the lattice constants of the zinc-blende ZnO and ZnS, respectively.

Next, we examine the mechanical behavior of $ZnS_{1-x}O_x$ compounds. We begin by calculating the elastic constants of these compounds by [31,32]:

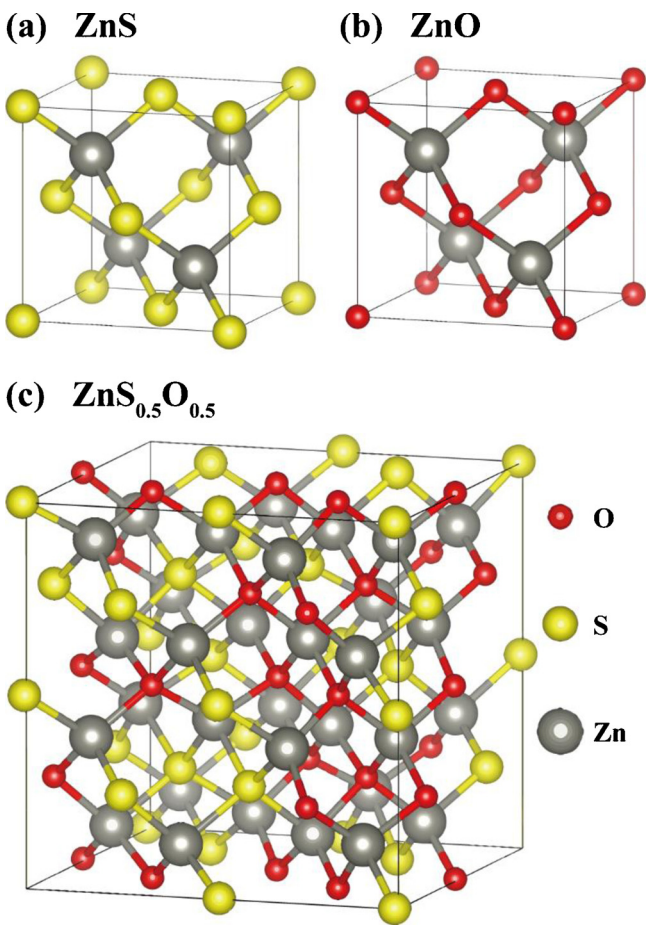

Fig. 1. The crystal structures of the zinc-blende phase of (a) pristine ZnS, (b) pristine ZnO, and (c) $ZnS_{0.5}O_{0.5}$ special quasi-random structures (SQS).

$$C_{ij} = \frac{1}{V_0}\frac{\partial^2 E}{\partial \zeta_i \zeta_j} \quad (2)$$

Where V_0 is the equilibrium volume of the cell. The second derivative of the total energy relative to the strains ($\frac{\partial^2 E}{\partial \zeta_i \zeta_j}$) can be determined by calculating the elastic response of the cell to the strain perturbations. We can then obtain three independent elastic constants for zinc-blende structures (C_{11}, C_{12}, and C_{44}). Fig. 2(b) outlines the elasti c constants of alloy $ZnS_{1-x}O_x$. In addition, the values of elastic constants for zinc-blende $ZnS_{1-x}O_x$ are listed in Table 1. It can be seen that these elastic constants increase near linearly as the oxygen concentration rises. The results for the magnitudes of C_{11}, C_{12}, and C_{44} in this work are also compatible with the previous literature [33–36]. The traditional mechanical stability criteria in cubic crystals are given by, $C_{11} > 0$, $C_{44} > 0$, $C_{11} > |C_{12}|$, $(C_{11}+2C_{12}) > 0$ [37]. According to the C_{11}, C_{12}, and C_{44} values for each superstructure of $ZnS_{1-x}O_x$ we constructed, the above criteria are satisfied for all $ZnS_{1-x}O_x$ compositions. It demonstrates that the zinc-blende structure of the $ZnS_{1-x}O_x$ system is thermodynamically stable.

Based on these obtained elastic constants, we can further derive bulk modulus (B), shear modulus (G), Young's modulus (E) and Poisson's ratio (υ) by the following [37,38]:

$$B = \frac{1}{3}(C_{11} + 2C_{12}) \quad (3)$$

$$G = \frac{1}{2}(G_V + G_R) = \frac{1}{2}\left[\frac{C_{11} - C_{12} + 3C_{44}}{5} + \frac{5(C_{11} - C_{12})C_{44}}{4C_{44} + 3(C_{11} - C_{12})}\right] \quad (4)$$

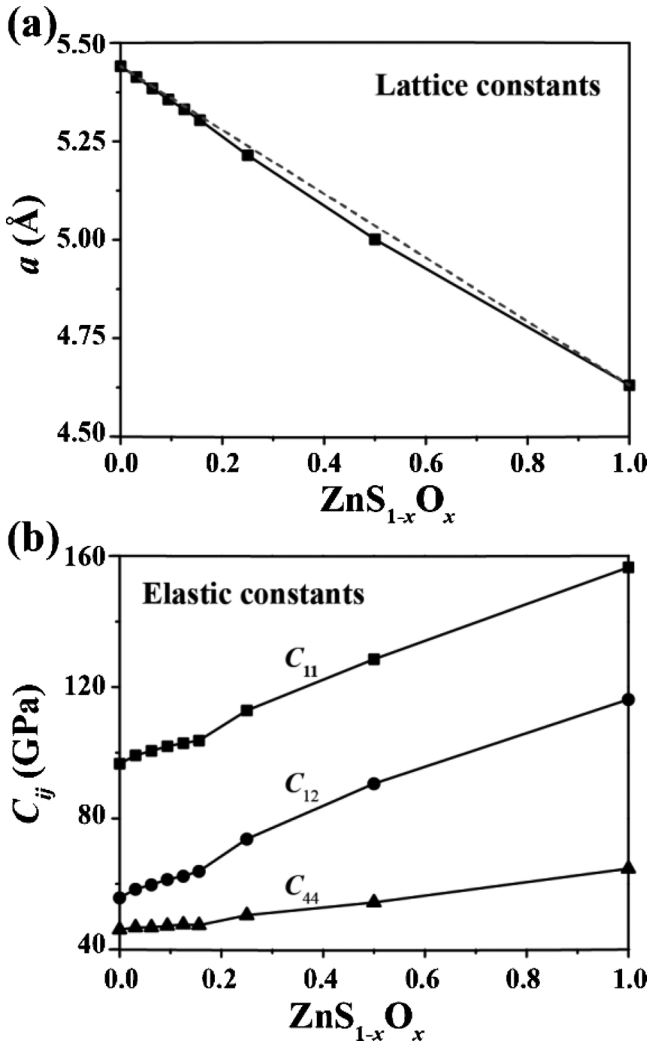

Fig. 2. The calculated (a) Lattice constants and (b) Elastic constants of $ZnS_{1-x}O_x$ compounds. The dashed line in (a) represents the Vegard's law as reference. (For interpretation of the references to color in this figure legend, the reader is referred to the web version of this article.)

$$E = \frac{9BG}{3B + G} \tag{5}$$

$$v = \frac{1}{2}\frac{3B - 2G}{3B + 2G} \tag{6}$$

Noted that the shear modulus (G) is from the Voigt-Reuss-Hill approximations [39]. It is a well-established scheme to determine the shear modulus of polycrystalline material by the arithmetic mean of the Reuss (G_V) and Voigt (G_R) extremes [40,41].

We can evaluate the effect of oxygen alloying in the system on the mechanical properties of $ZnS_{1-x}O_x$ compounds by plotting the changes of bulk modulus, shear modulus, Young's modulus and Poisson's ratio as a function of increasing oxygen concentration in Fig. 3. We first measure the resistance to the external deformation of $ZnS_{1-x}O_x$ compounds by examining the bulk modulus. We can see from Fig. 3(a) that the value of bulk modulus increases linearly with growing oxygen alloying. This indicates that the mechanical strength of ZnS is improved by adding oxygen as an alloying element. The effect of oxygen addition on the mechanical properties of $ZnS_{1-x}O_x$ compounds can be further observed in the change of Young's modulus and shear modulus, as shown in Fig. 3(b) and (c). Young's modulus is an indicator of a material's resistance to uniaxial stretching, and the shear modulus defines the resistance to shear forces. We can observe that both Young's modulus and shear modulus increase with the increasing oxygen content. These results demonstrate that doping oxygen into ZnS is beneficial for resisting the deformation caused by either uniaxial stretching or shear force. We can also imply that the oxygen alloying can improve the hardness of $ZnS_{1-x}O_x$ compounds since the hardness is normally positively correlated with the bulk modulus and the shear modulus [42]. Finally, the change of the Poisson's ratio associated with the oxygen content is shown in Fig. 3(d). Compared with ZnS, the doping oxygen increase the value of the Poisson's ratio, which indicates that the oxygen alloying can strengthen the response of $ZnS_{1-x}O_x$ compounds under loading. Overall, we can conclude that alloying oxygen can effectively improve the mechanical strength of ZnS.

3.2. Dielectric function and related optical properties

Now we turn to the optical properties of $ZnS_{1-x}O_x$ compounds. We first investigate the dielectric function $\varepsilon(\omega) = \varepsilon_1(\omega) + i\varepsilon_2(\omega)$ defining the relationship between the electrical and optical properties of materials, in which the frequency ω and the photon energy $E = \hbar\omega$ are given as the formalism by Ehrenreich and Cohen [43–45]. The imaginary part of the frequency-dependent dielectric function $\varepsilon_2(\omega)$ is given by [44,46–48]:

$$\varepsilon_2(\omega) = \frac{e^2\hbar}{\pi m^2\omega^2}\sum_{V,C}\int_{BZ} |M_{CV}(k)|^2\delta[\omega_{CV}(k) - \omega]d^3k \tag{7}$$

The integral was made over the first Brillouin zone. Here $M_{CV}(k)$ parameters are the dipolar matrix elements between valence band U_{Vk} and conduction band U_{Ck} states. $M_{CV}(k) = \langle U_{Ck}\,|e,\,\nabla|\,U_{Vk}\rangle$, where e is the polarization vector of the electric field, and $\hbar\omega_{CV}(k) = E_{Ck} - E_{Vk}$ is the excitation energy. Using the Kramers–Kronig relations, the real part $\varepsilon_1(\omega)$ can be derived from the imaginary part [48]:

$$\varepsilon_1(\omega) = 1 + \frac{2}{\pi}P\int_0^\infty \frac{\omega'\varepsilon_2(\omega')}{\omega'^2 - \omega^2}d\omega' \tag{8}$$

Where P represents the principal value of the integral.

The dielectric function is closely related to the optical properties of a material. With the real part and imaginary part of the dielectric function known, the primary optical properties, such as reflectivity and absorption coefficient can be derived. The explicit expressions of the reflectivity $R(\omega)$ (one-surface reflection from window materials in the air) and the absorption coefficient $I(\omega)$ are given by [49,50]:

$$R(\omega) = \left|\frac{\sqrt{\varepsilon(\omega)} - 1}{\sqrt{\varepsilon(\omega)} + 1}\right|^2 \tag{9}$$

$$I(\omega) = (\sqrt{2})\omega[\sqrt{\varepsilon_1(\omega)^2 + \varepsilon_2(\omega)^2}]^{1/2} \tag{10}$$

The total reflectivity (fraction of incident light reflected into the source) is derived from light reflected from both entry and exit surfaces, including contributions from multiple internal reflections. The total

Table 1
Elastic constants (GPa) for zinc-blende $ZnS_{1-x}O_x$.

x	0	0.03	0.06	0.09	0.13	0.16	0.25	0.50	1
C_{11}	96.64	99.17	100.52	101.95	102.93	103.69	112.9	128.53	156.52
C_{12}	55.79	58.39	59.77	61.37	62.41	63.83	73.71	90.58	116.26
C_{44}	46.1	46.73	46.74	47.2	47.6	47.43	50.48	54.38	64.7

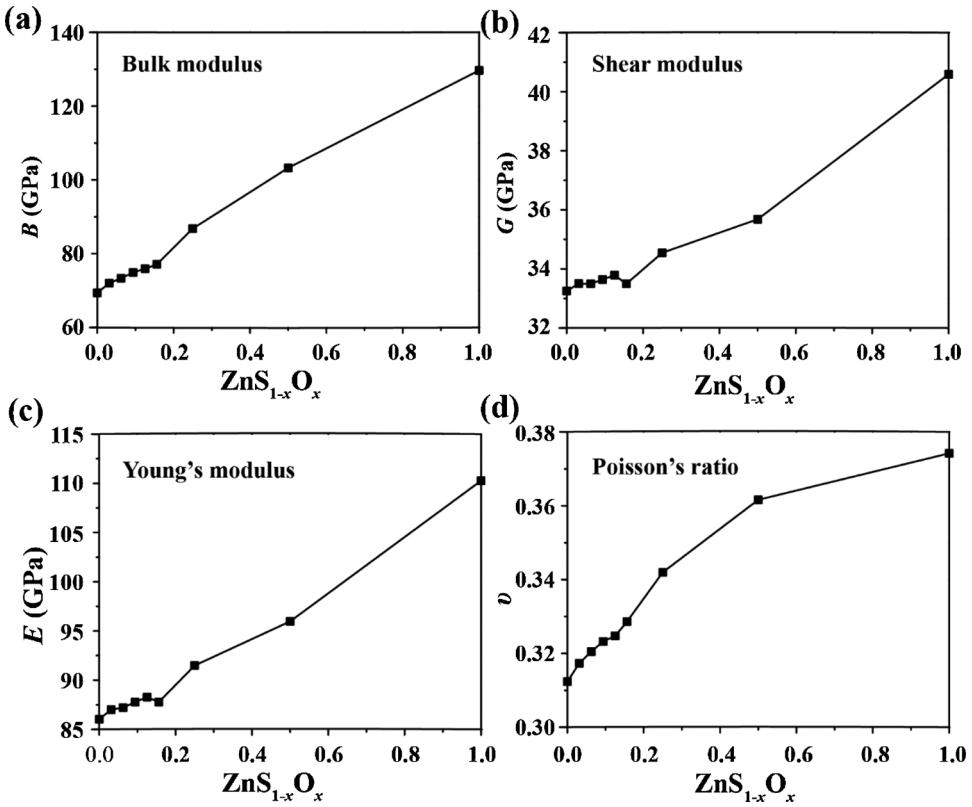

Fig. 3. The mechanical properties of $ZnS_{1-x}O_x$ compounds: (a) Bulk modulus; (b) Shear modulus; (c) Young's modulus; (d) Poisson's ratio.

reflectivity is given by [4]:

$$r(\omega) = \frac{2R(\omega)}{1 + R(\omega)} \tag{11}$$

Fig. 4(a) and (b) illustrate the calculated optical response functions, *i.e.*, the real part $\varepsilon_1(\omega)$ and the imaginary part $\varepsilon_2(\omega)$ of the dielectric function relative to the photon energy for different zinc-blende $ZnS_{1-x}O_x$ compositions, respectively. We find that the trends of the real (imaginary) part of the dielectric function with respect to the photon energy are similar for all $ZnS_{1-x}O_x$ alloys. For the real part $\varepsilon_1(\omega)$, the

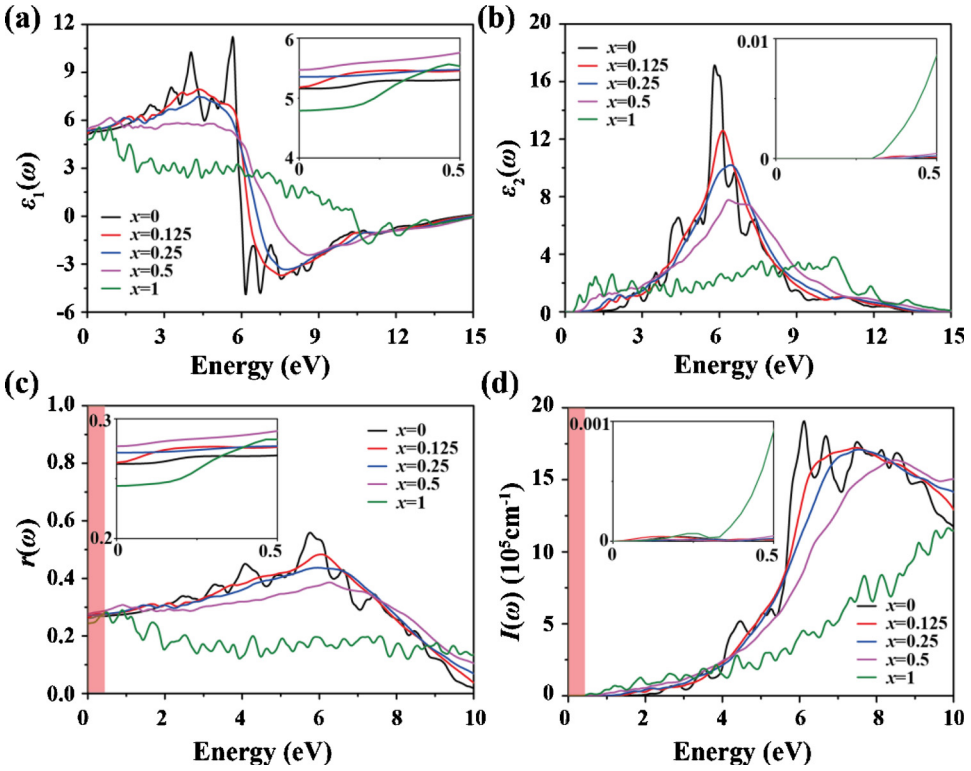

Fig. 4. The dielectric function and optical properties of $ZnS_{1-x}O_x$ compounds. (a) The real part, and (b) imaginary part of the dielectric function, (c) total reflectivity, and (d) absorption coefficient. The red bars in (c) and (d) represent the infrared region used for infrared window materials in real applications. (The insets show the red color range covering the mid-wave and long-wave infrared region.). (For interpretation of the references to color in this figure legend, the reader is referred to the web version of this article.)

multiple absorption peaks observed in the pristine ZnS disappears with the doping of oxygen. Noted that no significant change has been observed within the photon energy range from 0 to ~0.5 eV, *i.e.*, ε_1 is nearly constant within the infrared light window. In Fig. 4(b), the imaginary part curve of ZnS jumps at a critical point about 2.06 eV, which indicates the threshold for direct optical transitions between the valence band maximum and the first conduction band minimum, known as the fundamental absorption edge [51]. With the concentration of oxygen increasing, the absorption edge decreases. For the case of $ZnS_{0.5}O_{0.5}$ and ZnO, the values of critical points become 0.91 eV and 0.53 eV, respectively. It suggests that only the light with energy smaller than such critical value can pass through the material without absorption.

Fig. 4 (c) and (d) depict the total reflectivity (r(ω)) and the absorption coefficients ($I(\omega)$) as functions of photon energy, respectively. We focused on the Mid-infrared range corresponding to 0.248 – 0.413 eV of photon energy (for 3–5 μm midwave window), and the Far-infrared range corresponding to 0.088 – 0.155 eV of photon energy (for 8–14 μm longwave window), respectively [4]. We have found that the total reflectivity shows a steady trend for all oxygen concentrations (around 0.5 eV) investigated in both the mid-infrared region and the far-infrared region. Moreover, the absorption coefficient is not significantly affected by varying oxygen composition. It suggests that the optical properties of the pristine phase are nearly retained with oxygen alloying.

We have also evaluated the influence of oxygen alloying on the transmittance of the system. When the thickness b of the infrared window material is known, the transmittance (fraction of incident light transmitted) is given as below formula [4]:

$$T(\omega) = \frac{[1 - R(\omega)]^2 e^{-I(\omega)b}}{1 - [R(\omega)]^2 e^{-2I(\omega)b}} \tag{12}$$

Since the thickness of infrared window materials is usually within ~ μm scale in real applications [4], the relatively small value of absorption coefficients leads to the value of $e^{-2I(\omega)b}$ and $e^{-I(\omega)b}$ close to 1. Therefore, the following equation can be derived from Eq. (12) as:

$$T(\omega) = \frac{[1 - R(\omega)]^2}{1 - [R(\omega)]^2} = 1 - \frac{2R(\omega)}{1 + R(\omega)} = 1 - r(\omega) \tag{13}$$

It indicates that the effect of absorptivity in infrared area is small enough to be negligible for $ZnS_{1-x}O_x$ compounds so that the transmittance becomes one minus the total reflectivity. It is consistent with the results in previous literature [4,11]. As a result, the transmittance parameters of $ZnS_{1-x}O_x$ compounds are about 0.7 – 0.8 at 0.13 eV and 0.35 eV. Moreover, the transmittances within 0 – 0.5 eV of photon energy almost unchanged with the increase of oxygen concentration, indicating that doping oxygen elements into ZnS had little effect on the infrared window properties. It suggests that the synthesized $ZnS_{1-x}O_x$ compounds could be promising candidates for infrared window materials remaining good transmittance properties [29].

We can better understand the optical absorption properties of $ZnS_{1-x}O_x$ compounds by investigating the electronic band structure. Fig. 5 displays the calculated band structures of zinc-blende (a) ZnS, (b) $ZnS_{1-x}O_x$ (x = 0.5), and (c) ZnO along the representative directions of high symmetry points in the Brillouin zone. The calculated band gaps for pristine ZnS and ZnO are 2.02 eV and 0.60 eV, which are in accordance with previously calculated results (2.01 eV and 0.64 eV for ZnS and ZnO, respectively) [13,52]. Hence, the band gap of $ZnS_{1-x}O_x$ alloying compounds are in the range of 0.60 eV–2.02 eV. These are also consistent with the results of the imaginary part in the dielectric function and the absorption coefficients (Fig. 4(b) and (d)). Since PBE functional often underestimate the magnitude of band gap [53,54], these band structures are further checked using Heyd-Scuseria-Ernzerhof (HSE) screened-hybrid functional and PBE0 [55,56]. We find that except for the increased band gaps, the band features of HSE and PBE0 are consistent with that of PBE. The magnitude of PBE band gap

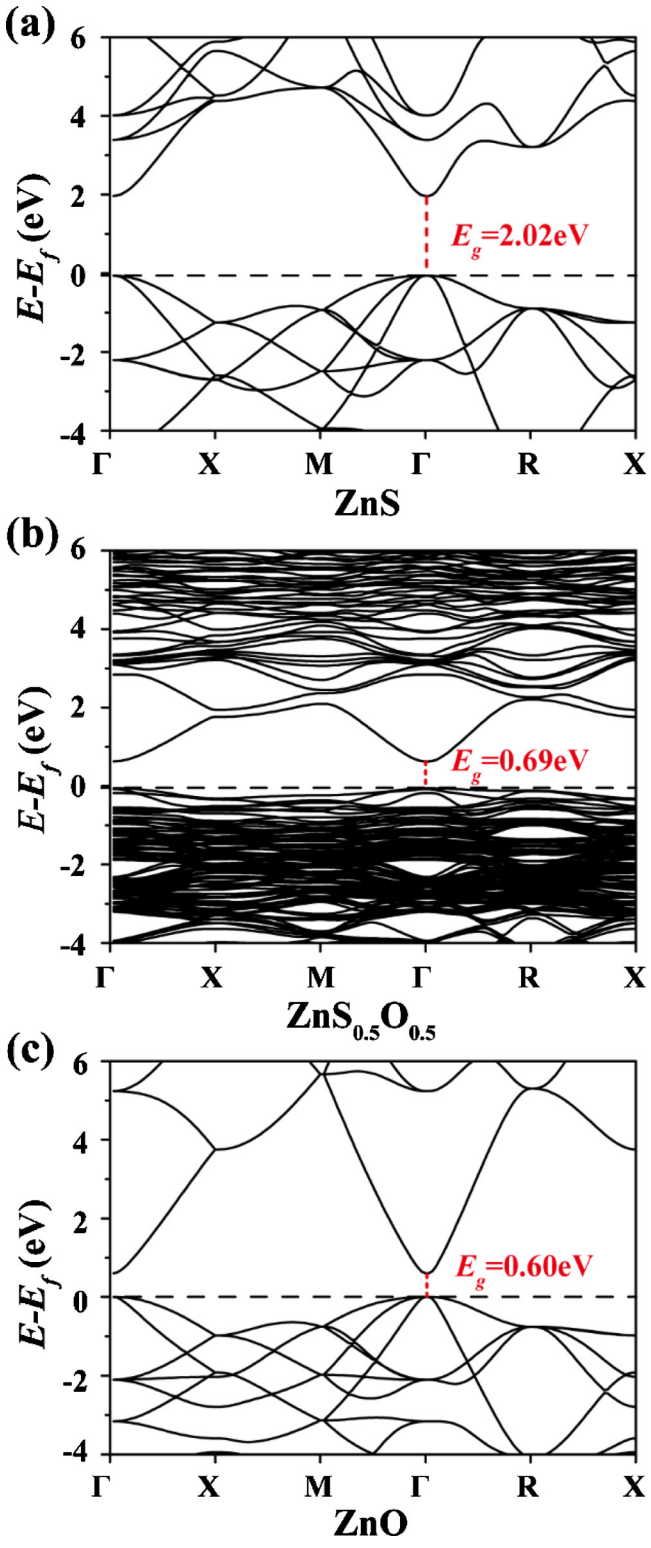

Fig. 5. Electronic band structures of (a) ZnS, (b) $ZnS_{0.5}O_{0.5}$, and (c) ZnO.

(0.60–2.02 eV) is larger than the midwave and long wave infrared window (< 0.5 eV) we focused on. Therefore, the magnitude of PBE band gap is sufficient not to induce electronic excitation to cause significant optical absorption to affect optical performance. We can then conclude that PBE can achieve reliable measurements on the evolution of optical properties in $ZnS_{1-x}O_x$ systems.

3.3. The effects of vacancy defects on the properties of $ZnS_{1-x}O_x$ compounds

Oxygen or sulfur vacancies are inevitable in oxide and sulfide structures during their fabrications. The presence of these vacancy defects can play an essential role in both the mechanical and optical properties of the $ZnS_{1-x}O_x$ system. We first studied the energetic feasibility of these vacancies by calculating the formation energy of vacancies for oxygen or sulfur atoms in $ZnS_{1-x}O_x$ compounds. The formation energy of vacancies is defined as [57]:

$$E_f = E(ZnS_xO_{1-x} + n \times V_X) + n \times E(X) - E(ZnS_xO_{1-x}) \quad (14)$$

Where $E(ZnS_xO_{1-x} + n \times V_X)$ is the energies of ZnS_xO_{1-x} with some vacancies by removing the X (O or S) atoms, n is the number of the vacancies, $E(X)$ is the cohesive energy of a single X (O or S) atom, and $E(ZnS_xO_{1-x})$ is the energy of ZnS_xO_{1-x} without vacancies.

Using the above equation, we examine the formation energy of oxygen vacancy and sulfur vacancy for $ZnS_{0.5}O_{0.5}$. The supercell, including 32 Zn atoms, 16 S atoms, and 16 O atoms, is employed. As such, the supercells of $ZnS_{0.5}O_{0.5}$ with different vacancy concentrations were constructed by the SQS method also [21]. The formation energies of V_S and V_O are determined as 1.85 eV per atom and 4.61 eV per atom, respectively. It suggests that sulfur vacancies are more energetic favorable to generate than oxygen vacancies.

Then we calculated the elastic constants and bulk modulus of $ZnS_{0.5}O_{0.5}$ with oxygen and sulfur vacancies, as shown in Fig. 6. Here c denotes the concentration of vacancy. The vacancy defects tend to reduce both the elastic constants and bulk modulus of $ZnS_{0.5}O_{0.5}$. Fig. 6(a) shows that the elastic modulus decreases slowly with the increase of sulfur vacancies. Relative with defect-free $ZnS_{0.5}O_{0.5}$, 12.5% concentration of sulfur vacancy reduces the C_{11} from 126.46 GPa to 110.68 GPa and decreases the C_{12} from 85.21 GPa to 57.22 GPa. Nevertheless, the elastic constant of C_{44} remains nearly unchanged. For oxygen vacancies, the change of the C_{12} and C_{44} keeps a similar trend with that of sulfur vacancies. However, the elastic constant C_{11} for oxygen vacancy cases exhibits a significant reduction compared with that for sulfur vacancy cases. The trend of bulk modulus illustrated in Fig. 6(b) provides more apparent evidence than elastic constants. For sulfur vacancies, the bulk modulus of $ZnS_{0.5}O_{0.5}$ decrease 7.45% for vacancy concentration of 6.25%, and 24.17% for vacancy concentration of 12.5%, respectively. However, the bulk modulus of $ZnS_{0.5}O_{0.5}$ with oxygen vacancies reduces dramatically. It decreases about 16.22% for 6.25% oxygen vacancies, and 34.69% for 12.5% oxygen vacancies. Therefore, we can conclude that the presence of oxygen vacancies leads to much degraded mechanical performance than sulfur vacancies.

Finally, we examine the optical properties of $ZnS_{0.5}O_{0.5}$ with oxygen vacancies and sulfur vacancies. The curves in Fig. 7(a) show the total reflectivity of $ZnS_{0.5}O_{0.5}$ with oxygen vacancies at different concentrations. For both mid-infrared and far-infrared light, the total reflectivity grows as the oxygen vacancy concentration increases. For comparison, Fig. 7(d) shows that the total reflectivity of $ZnS_{0.5}O_{0.5}$ with sulfur vacancies at different concentrations. Similar to the results of oxygen vacancies, sulfur vacancies also lead to an increase in the total reflectivity in the mid-infrared region and far-infrared region. Figs. 7(b) and (e) show the absorption coefficients of $ZnS_{0.5}O_{0.5}$ with oxygen vacancies and sulfur vacancies at different concentrations, respectively. It can be seen that the absorption coefficients of $ZnS_{0.5}O_{0.5}$ with vacancies are negligible within $0-0.5$ eV. Noted that the absorption coefficient of $ZnS_{0.5}O_{0.5}$ with 12.5% V_O becomes non-zero within 0.5–2.0 eV, as shown in Fig. 7(b). However, DFT calculations always underestimate the absolute value of the bandgap [49], causing the calculated absorption edges smaller than the experimental values. Hence it can be concluded that within both the midwave and longwave window, the vacancy has a negligible effect on the absorption coefficient of the $ZnS_{0.5}O_{0.5}$, and the absorption of light can be ignored. We observe a similar trend in the case of sulfur vacancies, as demonstrated in Fig. 7(e).

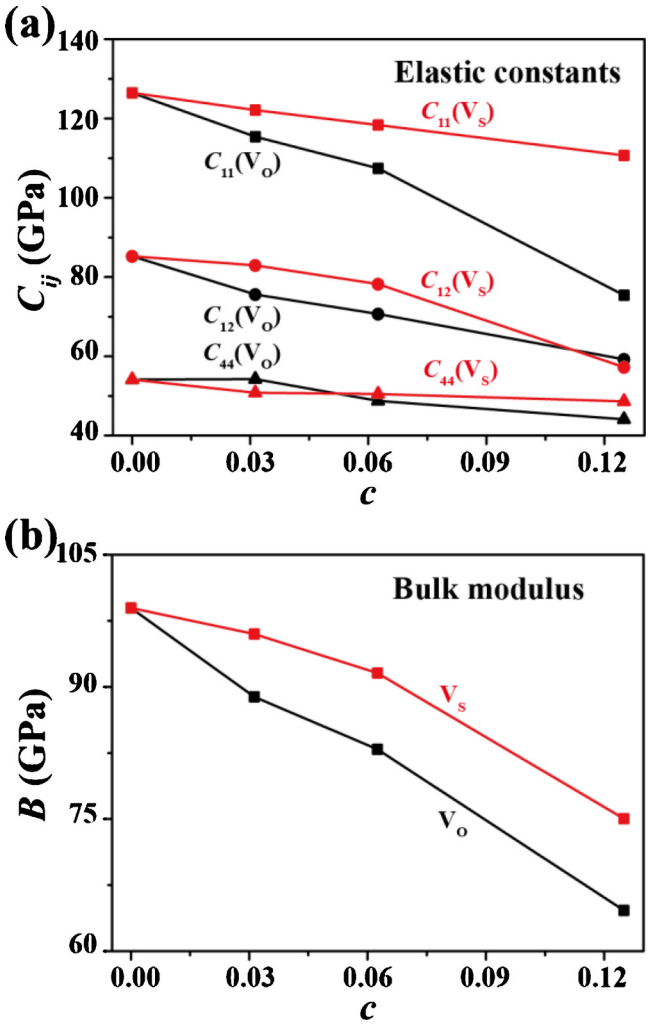

Fig. 6. The mechanical properties including (a) Elastic constants and (b) Bulk modulus of $ZnS_{0.5}O_{0.5}$ with oxygen vacancies or sulfur vacancies at different concentrations c.

Fig. 7(c) and 7(f) present the changes of total reflectivity and transmittance in $ZnS_{0.5}O_{0.5}$ with vacancy defects at a photon energy of 0.35 eV (Mid-infrared light) and 0.13 eV (Far-infrared light), respectively. Without considering the fraction of absorption, the transmittance of $ZnS_{0.5}O_{0.5}$ with oxygen or sulfur vacancies is considerably reduced with increasing vacancy concentrations. For example, Fig. 7(c) clearly show that the transmittance of the system is decreased by 12.59% compared to defectless composition when the oxygen vacancy concentration reaches 0.125 at 0.35 eV. Similarly, Fig. 7(f) reveals that the sulfur vacancies also decrease the transmittance of defect-free $ZnS_{0.5}O_{0.5}$ significantly. Therefore, we conclude that the generation of vacancy defects should be avoided during the preparation of $ZnS_{1-x}O_x$ compounds.

4. Conclusion

In summary, we have used first-principles calculations of structural, mechanical, and optical properties of the zinc-blende $ZnS_{1-x}O_x$ compounds. We have found that alloying oxygen into ZnS can improve the mechanical properties of materials effectively without reducing the transmittance in the infrared region. However, the presence of sulfur vacancies and oxygen vacancies in the system would weaken the mechanical strength as well as reducing the infrared optical transmittance of $ZnS_{1-x}O_x$ compounds. We suggest that the level of vacancy defects

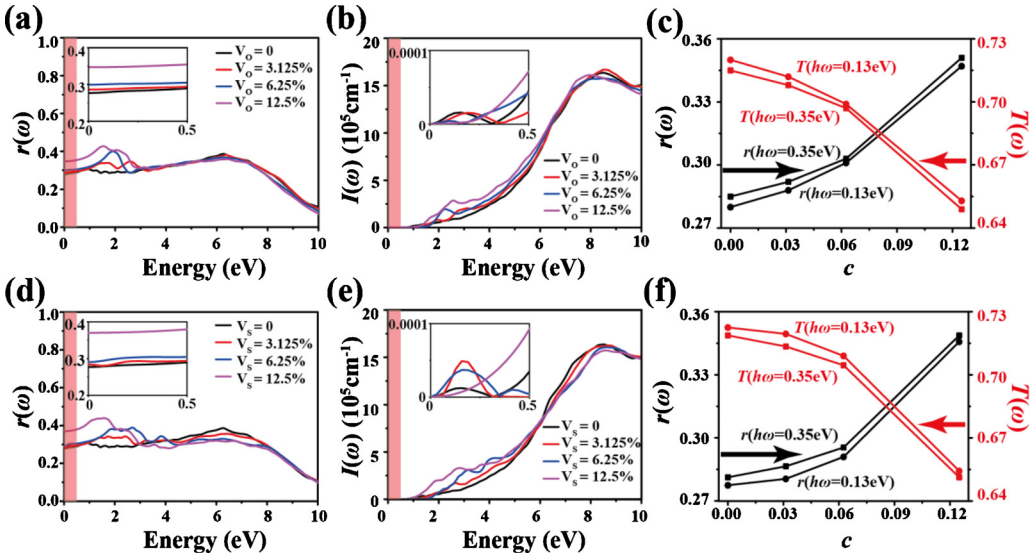

Fig. 7. The effect of vacancy defects on optical properties. (a) The total reflectivity, (b) the absorption coefficient, and (c) the variations of total reflectivity and transmittance for $ZnS_{0.5}O_{0.5}$ with oxygen vacancies at a photon energy of 0.35 eV (Mid-infrared light) and 0.13 eV (Far-infrared light); (d), (e), and (f) are the corresponding plots for $ZnS_{0.5}O_{0.5}$ with sulfur vacancies. The red bars represent the region used for infrared window materials. (The insets show the red color range covering the mid-wave and long-wave infrared region.). (For interpretation of the references to color in this figure legend, the reader is referred to the web version of this article.)

should be kept to a minimum during the fabrication of $ZnS_{1-x}O_x$ compounds. Therefore, we conclude that the alloying ZnO with ZnS can be a potential approach to achieve desirable infrared window materials with enhanced mechanical strength and good inferred optical properties, but in practice the structure needs to be carefully examined to reduce the detrimental effect of vacancy defects.

CRediT authorship contribution statement

Junfu Qi: Investigation, Writing - original draft. **Yuefeng Yin:** Data curation, Writing - review & editing. **Xiangdong Ding:** Resources. **Jun Sun:** Resources. **Junkai Deng:** Conceptualization, Writing - original draft, Writing - review & editing.

Declaration of Competing Interest

The authors declare that they have no known competing financial interests or personal relationships that could have appeared to influence the work reported in this paper.

Acknowledgments

The authors gratefully acknowledge the support of NSFC (Grant Nos.11974269, 51728203), and the support by 111 project 2.0 (Grant No. BP0618008). J. D. also thanks the support of National Key R&D Program of China (Grant No. 2018YFB1900104).

Appendix A. Supplementary data

Supplementary material related to this article can be found, in the online version, at doi:https://doi.org/10.1016/j.mtcomm.2020.101259.

References

[1] J. Zhu, J. Han, Infrared Antireflective and Protective Coatings, Walter de Gruyter GmbH & Co K.G., 2018.
[2] P. Yang, L. Liu, X. Zhang, J. Mo, Research progress of long-wavelength infrared optical materials, J. Inorg. Mater. 23 (2008) 641.
[3] C. Huang, J. Li, M. Lei, H. Du, Research progress and current trends in 3-5 micron optical materials, J. Synthetic Cryst. 32 (2003) 276.
[4] D.C. Harris, Materials for Infrared Windows and Domes: Properties and Performance, SPIE Press, 1999.
[5] J.R. Du, N.K. Chen, X.B. Li, S.Y. Xie, W.Q. Tian, X.Y. Wang, H.L. Tu, H.B. Sun, Exploring long-wave infrared transmitting materials with A_xB_y form: first-principles gene-like studies, Sci. Rep. 6 (2016) 21912.
[6] P. Klocek, Handbook of Infrared Optical Materials, Dekker, New York, 1991.
[7] J.A. Savage, Infrared Optical Materials and Their Antireflection Coatings, Bristol: Adam Hilger Ltd., 1985.
[8] C.A. Klein, Diamond windows and domes: flexural strength and thermal shock, Diamond Relat. Mater. 11 (2002) 218.
[9] X. Liu, J. Zhu, J. Han, Numerical and experimental investigation on thermal shock failure of Y_2O_3-coated CVD ZnS infrared windows, Int. J. Heat Mass Transfer. Theory Appl. (2018) 124 124.
[10] E.V. Yashina, Preparation and properties of polycrystalline ZnS for IR applications, Inorg. Mater. 39 (2003) 663.
[11] M. Liu, S. Wang, C. Wang, G. Zhang, Y. Wang, X. Li, P. Shang, R. Zhang, Y. Ji, J. Chu, Understanding of electronic and optical properties of ZnS with high concentration of point defects induced by hot pressing process: the first-principles calculations, Comput. Mater. Sci. 174 (2020) 109492.
[12] K. Hacini, H. Meradji, S. Ghemid, F. El Haj Hassan, Theoretical prediction of structural, electronic and optical properties of quaternary alloy $Zn_{1-x}Be_x$ S_ySe_{1-y}, Chin. Phys. B 21 (2012) 036102.
[13] D. Long, M. Li, D. Meng, Y. He, Electronic-structure and thermodynamic properties of $ZnS_{1-x}Se_x$ ternary alloys from the first-principles calculations, Comput. Mater. Sci. 149 (2018) 386.
[14] S. Hussain, L. Guo, H. Louis, S. Zhu, T. He, First-principles calculations of wurtzite $ZnS_{1-x}Se_x$ solid solutions for photocatalysis, Mater. Today Commun. 21 (2019) 100672.
[15] G.K. av, J. Furthmüller, Efficiency of ab-initio total energy calculations for metals and semiconductors using a plane-wave basis set, Comput. Mater. Sci. 6 (1996) 15.
[16] J.P. Perdew, K. Burke, M. Ernzerhof, Generalized gradient approximation made simple, Phys. Rev. Lett. 77 (1996) 3865.
[17] D.M. Ceperley, B.J. Alder, Ground state of the electron gas by a stochastic method, Phys. Rev. Lett. 45 (1980) 566.
[18] J.P. Perdew, A. Zunger, Self-interaction correction to density-functional approximations for many-electron systems, Phys. Rev. B 23 (1981) 5048.
[19] P.E. Blöchl, Projector augmented-wave method, Phys. Rev. B 50 (1994) 17953.
[20] G. Kresse, D. Joubert, From ultrasoft pseudopotentials to the projector augmented-wave method, Phys. Rev. B 59 (1999) 1758.
[21] A. Zunger, S. Wei, L.G. Ferreira, J.E. Bernard, Special quasirandom structures, Phys. Rev. Lett. 65 (1990) 353.
[22] A. van de Walle, Multicomponent multisublattice alloys, nonconfigurational entropy and other additions to the alloy theoretic automated toolkit, Calphad 33 (2009) 266.
[23] A. van de Walle, P. Tiwary, M. de Jong, D.L. Olmsted, M. Asta, A. Dick, D. Shin, Y. Wang, L.Q. Chen, Z.K. Liu, Efficient stochastic generation of special quasirandom structures, Calphad 42 (2013) 13.
[24] Y. Yu, J. Zhou, H. Han, C. Zhang, T. Cai, C. Song, T. Gao, Ab initio study of structural, dielectric, and dynamical properties of zinc-blende ZnX (X = O, S, Se, Te), J. Alloys. Compd. 471 (2009) 492.
[25] A. Ashrafi, C. Jagadish, Review of zincblende ZnO: stability of metastable ZnO phases, J. Appl. Phys. 102 (2007) 071101.
[26] A.B.M.A. Ashrafi, A. Ueta, A. Avramescu, H. Kumano, I. Suemune, Y.-W. Ok, T.-Y. Seong, Growth and characterization of hypothetical zinc-blende ZnO films on GaAs (001) substrates with ZnS buffer layers, Appl. Phys. Lett. 76 (2000) 550–552.
[27] S. Ves, U. Schwarz, N.E. Christensen, K. Syassen, M. Cardona, Cubic ZnS under pressure: optical-absorption edge, phase transition, and calculated equation of state, Phys. Rev. B 42 (1990) 9113.
[28] W.L. Bragg, F.R.S.J.A. Darbyshire, The structure of thin films of certain metallic oxides, Trans. Faraday Soc. 28 (1932) 522.
[29] S.K. Pandey, S. Pandey, A.C. Pandey, G.K. Mehrotra, Zinc oxysulfide ternary alloy nanocrystals: a bandgap modulated photocatalyst, Appl. Phys. Lett. 102 (2013) 233110.

[30] L. Vegard, Die konstitution der mischkristalle und die raumfüllung der atome, Z. Phys. 5 (1921) 17.
[31] S. Saib, N. Bouarissa, Ground-state and lattice dynamical properties of BeS in the zinc-blende and nickel arsenide phases, Solid State Sci. 12 (2010) 563.
[32] S. Saib, N. Bouarissa, P. Rodríguez-Hernández, A. Muñoz, Ab initio lattice dynamics and piezoelectric properties of MgS and MgSe alkaline earth chalcogenides, Eur. Phys. J. B 73 (2010) 185.
[33] R.A. Casali, N.E. Christensen, Elastic constants and deformation potentials of ZnS and ZnSe under pressure, Solid State Commun. 108 (1998) 793.
[34] A. Bellouche, A. Gueddim, S. Zerroug, N. Bouarissa, Elastic properties and optical spectra of $ZnS_{1-x}O_x$ dilute semiconductor alloys, Optik (2016) 11374.
[35] E. Güler, M. Güler, A theoretical investigation of the effect of pressure on the structural, elastic and mechanical properties of ZnS crystals, Braz. J. Phys. 45 (2015) 296.
[36] S.Q. Wang, A comparative first-principles study of ZnS and ZnO in zinc blende structure, J. Cryst. Growth 287 (2006) 185.
[37] Z. Wu, E. Zhao, H. Xiang, X. Hao, X. Liu, J. Meng, Crystal structures and elastic properties of superhard IrN_2 and IrN_3 from first principles, Phys. Rev. B 76 (2007) 054115.
[38] M. Friák, T. Hickel, B. Grabowski, L. Lymperakis, A. Udyansky, A. Dick, D. Ma, F. Roters, L.F. Zhu, A. Schlieter, U. Kühn, Z. Ebrahimi, R.A. Lebensohn, D. Holec, J. Eckert, H. Emmerich, D. Raabe, J. Neugebauer, Methodological challenges in combining quantum-mechanical and continuum approaches for materials science applications, Eur. Phys. J. Plus 126 (2011) 101.
[39] R. Hill, The elastic behaviour of a crystalline aggregate, Proc. Phys. Soc. Lond. Sect. A 65 (1952) 349.
[40] W. Voigt, Lehrbuch Der Kristallphysik, Teubner Leipzig, (1928).
[41] A. Reuss, Calculation of the flow limits of mixed crystals on the basis of the plasticity of monocrystals, Z. Angew. Math. Mech. 9 (1929) 49.
[42] D.M. Teter, Computational alchemy: the search for new superhard materials, MRS Bull. 23 (2013) 22.
[43] H. Ehrenreich, M.H. Cohen, Self-consistent field approach to the many-electron problem, Phys. Rev. 115 (1959) 786.
[44] A. Gueddim, S. Zerroug, N. Bouarissa, Optical characteristics of $ZnTe_{1-x}O_x$ alloys from first-principles calculations, J. Lumin. 135 (2013) 243.
[45] A. Soni, K.C. Bhamu, J. Sahariya, Investigating effect of strain on electronic and optical properties of lead free double perovskite $Cs_2AgInCl_6$ solar cell compound: a first principle calculation, J. Alloys. Compd. 817 (2020) 152758.
[46] M.A. Khan, A. Kashyap, A.K. Solanki, T. Nautiyal, S. Auluck, Interband optical properties of Ni_3Al, Phys. Rev. B 48 (1993) 16974.
[47] C. Koenig, M.A. Khan, Self-consistent electronic structure of FeAl, Phys. Rev. B 27 (1983) 6129.
[48] Z. Charifi, H. Baaziz, A. Hussain Reshak, Ab-initio investigation of structural, electronic and optical properties for three phases of ZnO compound, Phys. Status Solidi B 244 (2007) 3154.
[49] S.Z. Karazhanov, P. Ravindran, A. Kjekshus, H. Fjellvåg, B.G. Svensson, Electronic structure and optical properties of ZnX (X = O, S, Se, Te): a density functional study, Phys. Rev. B 75 (2007) 155104.
[50] H. Shi, M. Chu, P. Zhang, Optical properties of UO_2 and PuO_2, J. Nucl. Mater. 400 (2010) 151.
[51] N. Bouarissa, The effect of hydrostatic pressure on the electronic and optical properties of InP, SolidState Electron. 44 (2000) 2193.
[52] A. Schleife, F. Fuchs, J. Furthmüller, F. Bechstedt, First-principles study of ground- and excited-state properties of MgO, ZnO, and CdO polymorphs, Phys. Rev. B 73 (2006) 245212.
[53] D. Sholl, J.A. Steckel, Density Functional Theory: a Practical Introduction, John Wiley & Sons, 2011.
[54] R. Laskowski, N.E. Christensen, Ab initiocalculation of excitons in ZnO, Phys. Rev. B 73 (2006) 045201.
[55] J. Heyd, G.E. Scuseria, M. Ernzerhof, Hybrid functionals based on a screened Coulomb potential, J. Chem. Phys. 118 (2003) 8207.
[56] J. Paier, R. Hirschl, M. Marsman, G. Kresse, The Perdew–Burke–Ernzerhof exchange-correlation functional applied to the G2-1 test set using a plane-wave basis set, J. Chem. Phys. 122 (2005) 234102.
[57] L. Chen, Z. Hou, Z. Zhu, Y. Yang, First-principles calculation of the vacancy formation energies in LiAl, Acta Phys. Sin. 52 (2003) 2229.